Catalysis Today 453 (2025) 115262

Contents lists available at ScienceDirect

Catalysis Today

journal homepage: www.elsevier.com/locate/cattod

Optimizing Sorption Enhanced Methanation (SEM) of CO_2 with Ni_3Fe + LTA 5 A mixtures

V.D. Mercader, P. Aragüés-Aldea, P. Durán, E. Francés, J. Herguido, J.A. Peña *

Catalysis and Reactor Engineering Group (CREG) - Aragon Institute of Engineering Research (I3A) Universidad Zaragoza, c/ Mariano Esquillor s/n, Zaragoza 50018, Spain

ARTICLE INFO

Keywords:
Methanation
CO_2 utilization
Biogas upgrading
Adsorption-enhanced methanation
LTA zeolite
Renewable hydrogen
biomethane

ABSTRACT

This study investigates the integration of catalytic CO_2 methanation and water adsorption using a Ni-Fe-based catalyst and LTA 5 A zeolite to enhance methane production via the Sabatier reaction. By mitigating thermodynamic limitations through *in situ* water removal, the research explores key operational parameters, including temperature, space velocity, and H_2:CO_2 feed ratios, to optimize process performance. The findings highlight that a temperature of 300 °C, a *WHSV* of 1.50×10^4 (STP) $mL \cdot g_{cat}^{-1} \cdot h^{-1}$ (4.86 $g_{CO2} \cdot g_{cat}^{-1} \cdot h^{-1}$), and a H_2:CO_2 molar ratio equal to 5:1, result in enhanced methane yields, shifting thermodynamic equilibrium due to water sorption during initial stages. The presence of methane in the feed, representative of a biogas, demonstrated negligible effects on methane yields under optimal conditions, underscoring the method's feasibility for direct biogas upgrading. While the process achieved significant intensification, challenges such as loss of activity of the bed of solids (catalyst plus water adsorbent) were identified, necessitating further advancements in both catalyst and adsorbent stability, as well as a deeper study on their interaction. The study provides a pathway for scaling up adsorption-enhanced methanation technologies to achieve renewable methane production, addressing the dual goals of carbon management and energy storage.

1. Introduction

The global transition toward renewable energy and the need for sustainable chemical processes have driven significant interest in the development of efficient carbon dioxide (CO_2) utilization technologies. Among these, catalytic methanation—a process that converts CO_2 and hydrogen (H_2) into methane (CH_4)—has emerged as a versatile approach for renewable energy storage and carbon recycling [1,2]. Methane, the principal component of natural gas, offers an energy-dense and clean fuel alternative that seamlessly integrates with existing natural gas infrastructure, including pipelines, storage facilities, and combustion systems. This adaptability makes methane production through catalytic methanation an attractive avenue for sustainable energy applications [3]. Furthermore, methanation serves as the cornerstone of *Power-to-Gas* (PtG) technologies, which store surplus renewable electricity—generated from intermittent sources such as solar or wind—as Synthetic Natural Gas (SNG). This integration addresses the dual challenges of energy storage and decarbonization by leveraging renewable electricity to produce storable and transportable chemical fuels [4,5].

The *Sabatier* reaction, which underpins catalytic methanation, is a highly exothermic and equilibrium-limited reaction (r.1). While thermodynamically favorable at moderate temperatures, achieving high methane yields is challenging due to the competing reverse water-gas shift (RWGS) reaction (r.2) and the sensitivity of reaction kinetics and equilibrium to operating conditions [6,7]. The accumulation of water, a byproduct of methanation, further exacerbates these challenges by inhibiting reaction equilibrium and catalyst performance. Strategies for removing water in situ have gained attention as an effective means to shift the equilibrium toward higher CH_4 yields, thereby intensifying the process [8].

$$CO_2 + 4H_2 \rightleftharpoons CH_4 + 2H_2O \quad \Delta H_r^0 = -165.1 \left[kJ \cdot mol^{-1}\right] \tag{r.1}$$

$$CO_2 + H_2 \rightleftharpoons CO + H_2O \quad \Delta H_r^0 = +41.2 \left[kJ \cdot mol^{-1}\right] \tag{r.2}$$

$$CO + 3H_2 \rightleftharpoons CH_4 + H_2O \quad \Delta H_r^0 = -206.3 \left[kJ \cdot mol^{-1}\right] \tag{r.3}$$

Among the emerging intensification strategies, integrating water adsorption directly within the catalytic methanation process has shown great promise. By employing sorption-enhanced methodologies such as

* Correspondence to: Aragon Institute of Engineering Research (I3A); Universidad Zaragoza; c/ Mariano Esquillor s/n; Zaragoza 50018, Spain.
E-mail address: jap@unizar.es (J.A. Peña).

https://doi.org/10.1016/j.cattod.2025.115262
Received 10 January 2025; Received in revised form 25 February 2025; Accepted 2 March 2025
Available online 10 March 2025

the *Sorption-Enhanced Sabatier Reaction* (SESaR) or *Sorption-Enhanced Methanation* (SEM), materials like zeolites can selectively adsorb water, driving the equilibrium toward higher methane production under milder reaction conditions [9]. This approach, grounded in *Le Châtelier* principle, offers new opportunities to improve process efficiency, provided that the adsorbents, catalysts, and operating parameters are carefully optimized [10].

Nickel-based catalysts are preferred for methanation due to their high activity, affordability, and availability [11,12]. Recent studies suggest that incorporating iron as a co-catalyst with nickel can enhance catalytic performance by improving resistance to sintering and oxidation while broadening operational stability [13]. Furthermore, the use of low-silica zeolites, such as LTA frameworks, has demonstrated strong water adsorption capabilities that are critical for process intensification [14]. The synergy between nickel-iron (Ni-Fe) catalysts and zeolite-based adsorbents has been the subject of increasing interest [15], as it effectively couples catalytic activity with water removal to overcome equilibrium limitations and maximize CH_4 yields [16].

Building upon these advancements, this study explores a bimetallic Ni:Fe catalyst (3:1 wt ratio) paired with zeolite LTA 5 A as a sorbent as continuation of previous research from Mercader *et al.* [17]. Preliminary research by the CREG group has demonstrated the potential of Ni-Fe catalysts to achieve superior methane selectivity and conversion compared to conventional nickel or ruthenium catalysts [18]. Combining these findings with the intensification potential of zeolite LTA 5 A adsorption, as previously reported by Gómez *et al.* [19] and Cañada-Barcala *et al.* [20], this research seeks to advance the understanding of catalytic-adsorptive methanation.

This study systematically investigates the effects of key operating parameters -such as H_2:CO_2 feed ratios, volumetric flow rates, and catalyst-to-adsorbent ratios- on the performance of an intensified methanation system. The work also examines the challenges associated with catalyst and adsorbent stability under reaction conditions, providing insights into the trade-offs between enhanced performance and long-term operability. The results aim to inform the design of scalable processes that integrate adsorption-based intensification, contributing to the growing demand for renewable methane production while addressing global challenges in carbon management and energy storage.

2. Experimental setup

2.1. Solids

These experiments were done using a Ni (7.5 ^{w}%) and Fe (2.5 ^{w}%) solid catalyst, to generate methane, and an LTA zeolite for water adsorption. The catalyst was prepared through incipient wetness impregnation, using γ-Al_2O_3 (*Sasol PURALOX*) as a support and hydrated nickel and iron nitrates (*Sigma Aldrich*) as precursors of both active phases. After impregnation, the samples were dried for 24 hours and calcined, for 1 hour, at 500 °C. Finally, the obtained solid was sieved, in order to use particles with a diameter between 100 and 200 μm. This catalyst is highly active and selective, allowing the achievement of high yields towards methane, which can then be pushed further to overcome thermochemical limitations when combined with water adsorption (*Le Châtelier* principle) and intensify the reaction process.

Several characterization techniques were applied to the solids, including N_2 adsorption-desorption isotherms (BET), X-Ray fluorescence for composition (XRF) and X-Ray diffraction (XRD) for the identification of crystalline structures in the catalyst and the zeolite. Temperature programmed reduction (TPR) (β= 5 °C/min) was only used for the catalyst with a H_2/N_2 flow of 100 (STP) mL·min^{-1} and hydrogen partial pressure of 0.05 bar out of 1 bar of total pressure. SEM-EDX technique was used to evaluate the proper dispersion of the active phase and the particle shape. BET results showed that the impregnation of metals on the surface and later calcination of the catalyst provoked a slight decrease in the surface area respecting to the fresh γ-Al_2O_3. The characterization details can be consulted in a previous study reported by V. D. Mercader *et al.* [17]. Results of TPR demonstrated that the addition of Fe produced a decrease in the reduction temperature at 350 °C for the Ni/Fe alloy [17,18].

The effect of diffusional constraints (internal and external) was also studied, fixing a minimum (constant) volumetric flowrate of 125 (STP) mL·min^{-1}, and a particle size between 100 and 250 μm (for both catalyst and zeolite). Both aspects ensure kinetic regime control.

Water adsorption was achieved using a commercial (*Alfa Aesar*) LTA 5 A zeolite, which is crushed and sieved in order to use a particle diameter of 100–200 μm. Its small pore diameter should make it ideal for these experiments, allowing selective removal of water (particle size of 2.8 Å) with small interference of other substances. Experimental tests were carried out by Thermogravimetric Analysis (TGA) at experimental temperatures and partial pressures of H_2O:CO_2 mixtures in the feeding. The TGA device was a Simultaneous Thermal Analysis System (STA), model *STA 449 F1 Jupiter-NETZSCH*. TGA results demonstrate that water adsorption is strongly favored over that of carbon dioxide and methane. Table 1 depicts adsorption equilibrium for water, while Table 2 compares adsorption capacities for methane and carbon dioxide. In addition, the high specific surface area of the zeolite (428 $m^2 \cdot g^{-1}$) and its low Si/Al ratio (1.087) makes it a good option for water adsorption.

2.2. Reaction experiments

The experiments were carried out using a conventional, quartz-made (ϕ_{in} = 13 mm) vertical fixed-bed reactor (as seen in Fig. 1), operating at atmospheric pressure. Prior to the beginning, the catalytic bed was prepared by mixing both solids (i.e., the catalyst and zeolite) in the indicated proportions. After emptying the reactor and filling it again with the new bed, it was heated up to 500 °C and reduced with hydrogen (2 hours). The experiment took place after cooling down to the reaction temperature; both the heating up and cooling were carried out in an inert atmosphere.

The analyzed parameters and operating conditions can be seen in Table 3. The temperature profile along the reactor was measured and registered using five thermocouples, located at different heights (1, 3, 6, 9, and 12 cm) above the support plate that sustained the solids bed, and its effect on results was also considered. Exhaust gases coming out from the reactor were first conducted to a cold trap (*Peltier* module) where water was condensed (thus avoiding damage to the analysis system), and then to a micro gas chromatograph (*Agilent 490 Micro GC*) to determine their compositions.

This research began with the study of space velocities in reaction performance with the aim of achieving an optimal yield value that should result in significant water formation. They were followed by an analysis of reaction temperature and partial pressures, which are expected to have a significant influence on adsorption and water generation, respectively.

The bed of solids introduced into the reactor was composed of a) the catalyst, with a variable load (1 g when analyzing reaction temperatures and partial pressures) and the b) zeolite (or silicon carbide used as inert). The total mass of solid (i.e., catalyst and zeolite/SiC) was set at 10.5 g. The temperature was modified from 250 to 400 °C in increments of 50 °C. Partial pressures or molar ratios H_2:CO_2, varied between 2:1, 3:1,

Table 1
Water adsorption equilibrium, at different temperatures and partial pressures. Overall pressure: 1 bar Results in g_{H2O}/100 $g_{zeolite}$.

	T (oC)	*250*	*300*	*325*	*350*	*400*
p_{H2O} (bar)	0.05	2.06	1.10	0.83	0.62	0.36
	0.08	2.54	1.48	1.07	0.85	0.55
	0.10	2.87	1.65	1.19	0.93	0.58
	0.12	2.92	1.72	1.34	1.03	0.78

Table 2
Carbon dioxide and methane adsorption equilibrium, at different temperatures. Partial pressure: 0.40 bar. Overall pressure: 1 bar. Results in g_{CO2} or $g_{CH4}/100\ g_{zeolite}$.

	T(°C)	*250*	*300*	*350*	*400*
Gas	CO_2	0.61	0.27	0.18	0.10
	CH_4	0.19	0.11	0.25	0.15

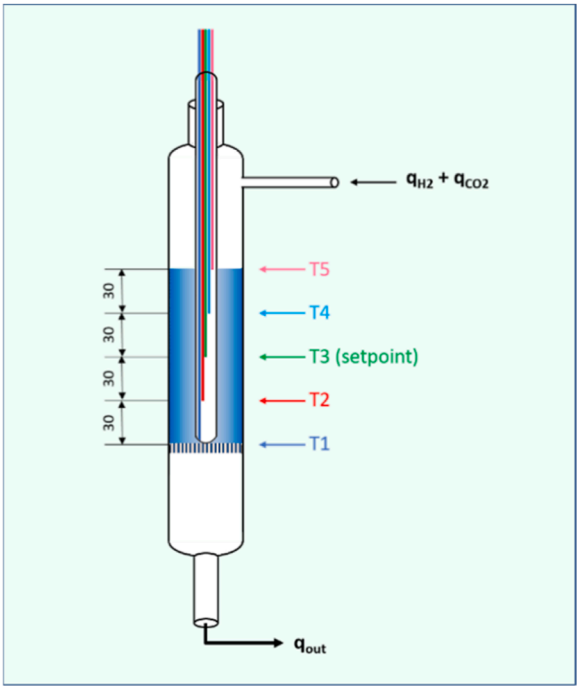

Fig. 1. Reactor sketch, along with the thermocouples used to measure temperature profiles. Total height: 50 cm. Inner diameter: 13 mm. Thermocouples at heights: 12, 9, 6 (oven control), 3, and 1 cm above distribution plate.

Table 3
Parameters and operating conditions.

	Standard value	*Interval*
Catalyst load, $W_{cat,0}$ (g)	1	0.125 – 1
Total gas flow, q_0 ((STP) mL·min^{-1})	250	125 – 250
H_2:CO_2 molar ratio	4:1	2:1 – 6:1
CH_4:CO_2 molar ratio	7:3	0 – 7:3
Temperature set-point (°C)	350	250 – 400
Total pressure (bar)	1	–
Total bed weight (catalyst + zeolite) (g)	10.5	–

4:1, 5:1 and 6:1. All experiments were performed at ambient pressure. When analyzing the presence of methane in the feeding, the CH_4:CO_2:H_2 ratio was kept in 7:3:12, simulating a sweetened biogas with ratio CH_4:CO_2 = 7:3 and a stoichiometric proportion of H_2:CO_2 equal to 4:1. Finally, two experiments were carried out, using silicon carbide instead of zeolite, in order to quantify the degree of intensification achieved in the presence of an adsorbent.

Prior to carrying out the experiments, the catalyst was activated at 500 °C for 2 hours (using a total flow of 250 (STP) mL·min^{-1}, with a 50 ^{v}% of H_2, 45 ^{v}% Ar, and 5 ^{v}% N_2). An experiment consists of five stages, in which conversion and selectivity are measured to detect existent intensifications. The first, third, and fifth stages (named in the next chapter as M_1, M_2, and M_3, standing for the first, second and third methanation stages) lasted for 1 hour. Along the reaction stages, a mixture consisting of 5 ^{v}% Ar, 5 ^{v}% N_2, and H_2, CH_4, and CO_2 in their respective proportions, was fed to the bed of catalyst and zeolite, resulting in the simultaneous reaction and removal of water by zeolite from the reaction environment. The second and fourth stages (named D_1 and D_2, standing for the first and second desorption stages) were carried out in order to desorb water from the zeolite and to analyze their effectiveness. The sweeping flow was 125 (STP) mL·min^{-1}, composed by 90 ^{v}% Ar and 10 ^{v}% N_2. The D_1 stage took place at the same temperature as the reaction stages and lasted for 30 minutes, while D_2 took place for 10 minutes at 500 °C (plus the heating up and cooling down to the reaction temperature).

After determining the exhaust gas composition, the molar flows of each compound were calculated (with N_2 as an internal standard) along with conversions of carbon dioxide and hydrogen (x_{CO_2} and x_{H_2}, Eqs. 1 and 2) and yields to each reaction product (carbon monoxide and methane) ($Y_{CO_2\to CH_4}$ and $Y_{CO_2\to CO}$, Eqs. 3 and 4).

$$CO_2\ conversion\ (-) = x_{CO_2} = \left[\frac{\left(f_{CO}|_{out} + f_{CH_4}|_{out} - f_{CH_4}|_{in}\right)}{\left(f_{CO}|_{out} + f_{CH_4}|_{out} + f_{CO_2}|_{out}\right)}\right] \quad (1)$$

$$H_2\ conversion\ (-) = x_{H_2} = \left[\frac{\left(f_{H_2}|_{in} - f_{H_2}|_{out}\right)}{f_{H_2}|_{in}}\right] \quad (2)$$

$$CH_4\ yield\ (-) = Y_{CO_2\to CH_4} = \left[\frac{\left(f_{CH_4}|_{out} - f_{CH_4}|_{in}\right)}{\left(f_{CO_2}|_{in}\right)}\right] \quad (3)$$

$$CO\ yield\ (-) = Y_{CO_2\to CO} = \left[\frac{\left(f_{CO}|_{out}\right)}{\left(f_{CO_2}|_{in}\right)}\right] \quad (4)$$

In these last four equations, $f_k|_{in}$ and $f_k|_{out}$ are total molar flows (mmol·min^{-1}) of the compound k entering or leaving the reactor, respectively. Since the only considered products were CO and CH_4, the addition of their yields is equal to the CO_2 conversion. Furthermore, the addition of the three exhaust gas flows (CH_4, CO, and CO_2) was compared to that of the inlet gas flows, in order to check that the experiments are correctly performed and parameters calculated. Intensifications of the process, meanwhile, are calculated with (Eqs. 5 and 6), with stable values ($Y^{stable}_{CO_2\to CH_4}$) being those achieved at the end of the stage (with a saturated zeolite, which leads to reaching a steady state). Results also require multiplying by 2 (as two moles of water are formed per mol of methane). Although carbon monoxide was also present in the reactor outlet, yields to this gas were very low when compared to those towards methane (only in one specific case, at the highest space velocity (shown in Fig. 2) did results of this parameter rise above 0.015, reaching a maximum of 0.023). Thus, they were not considered for measurement of intensifications.

$$Specific\ intensifications\left(\frac{adsorbed\ mmol\ of\ water}{kg_{zeolite}}\right) = \frac{f_{CO_2}|_{in}\cdot\int_0^t 2\cdot\left(Y_{CO_2\to CH_4} - Y^{stable}_{CO_2\to CH_4}\right)\cdot dt}{W_{zeolite}} \quad (5)$$

$$Relative\ intensifications(adim) = \frac{\int_0^t 2\cdot\left(Y_{CO_2\to CH_4}\right)\cdot dt}{\int_0^t 2\cdot\left(Y^{stable}_{CO_2\to CH_4}\right)\cdot dt} \quad (6)$$

3. Results and discussion

3.1. Influence of space velocity (WHSV) in methane and water generation

The first step consisted in reaction experiments modifying catalyst loads (W_{cat}) and reactants flows (q_0) while keeping a constant bed weight (10.5 g). Thus, space velocity was changed while keeping a constant carbon dioxide concentration (18 ^{v}%) in the feed stream to the

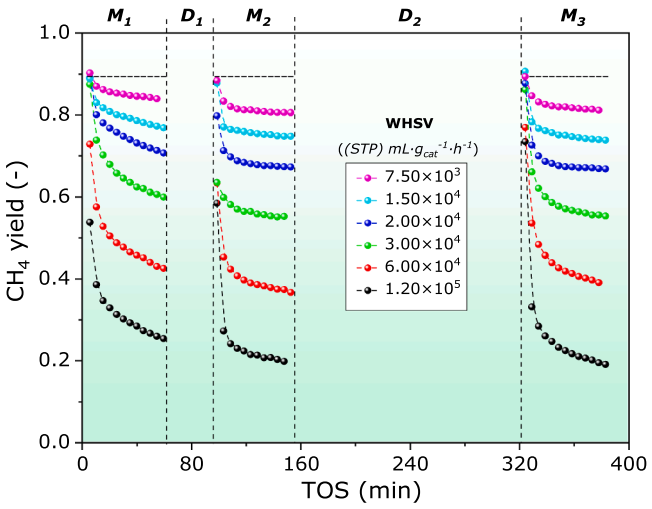

Fig. 2. Methane yield ($Y_{CO_2 \rightarrow CH_4}$) at different space velocities (*WHSV*) along methanation (M) + desorption (D) experiments. H_2:CO_2 molar ratio = 4:1. Reactants: Inert molar ratio = 9:1. T = 350 °C. Total bed load: 10.5 g. Horizontal dashed lines represent thermodynamic equilibrium conversion calculated by ΔG minimization.

reactor. It is important noting that the reduction of the amount of catalyst was compensated by the increase in zeolite content. Fig. 2 displays the different yields achieved when analyzing the influence of this parameter.

Firstly, W_{cat} was modified from 0.125 to 1 g, while the total flowrate was kept constant at 250 (STP) mL·min^{-1} (WHSV from 1.2 ×10^5 to 1.5 ×10^4 (STP) mL·g^{-1}·h^{-1}). Secondly, q_0 was varied from 250 to 125 (STP) mL·min^{-1}, with a constant W_{cat} of 1 g (WHSV = 7.5 ×10^3 (STP) mL·g^{-1}·h^{-1}). Experimental results demonstrate that, generally, smaller space velocity values lead to higher amounts of water being formed and adsorbed into the zeolite. The best situation in terms of stability and total amount of water produced was reached with W_{cat} = 1 g and q_0 = 250 (STP) mL·min^{-1} (*WHSV* = 1.50 ×10^4 (STP) mL·g$^{-1}_{cat}$·h^{-1}).

It is confirmed that, as it could be expected, a lower space velocity (or greater contact time) results in higher yields to methane. As such, when operating at *WHSV* = 1.20 × 10^5 (STP) mL·g$^{-1}_{cat}$·h^{-1} (the highest value), yields tends to stabilize in around $Y_{CO_2 \rightarrow CH_4}$ = 0.2, while working at *WHSV* = 1.50 × 10^4 and 7.50 × 10^3 (STP) mL·g$^{-1}_{cat}$·h^{-1} leads to yields $Y_{CO_2 \rightarrow CH_4}$ in the nearby of 0.8 -close to the thermochemical equilibrium-. In addition, in the initial steps (i.e., when the zeolite is still not saturated and water adsorption favors the reaction process) for the three lowest *WHSV* values, this thermodynamical threshold value is slightly overcome, and results are located at $Y_{CO_2 \rightarrow CH_4}$ > 0.9. It can also be observed that, in this situation, stable values are reached earlier: stabilization is sooner and so it is the saturation with water of the zeolite. This is explained as the consequence of higher amounts of water being formed and adsorbed by zeolite when *WHSV* gets lower (from 1.2 ×10^5 to 1.5 ×10^4 (STP) mL·g$^{-1}_{cat}$·h^{-1}). Thus, when water formation is favored, the zeolite saturates at an earlier time on stream and intensification process ceases more abruptly; something that, at shorter contact times (i.e., higher *WHSV*), happens gradually.

However, Fig. 2 also shows that, once *WHSV* reaches 1.50 × 10^4 (STP) mL·g$^{-1}_{cat}$·h^{-1}, yields do become stable (which means that the zeolite becomes saturated) and do not rise significantly when operating at a lower rate value (7.50 ×10^3 (STP) mL·g$^{-1}_{cat}$·h^{-1}). Another issue that should be noted is that, when testing the lower *WHSV* value (7.50 ×10^3 (STP) mL·g$^{-1}_{cat}$·h^{-1}), total reactants flowrate (q_0) was modified instead of the catalyst load (W_{cat}), from 250 to 125 (STP) mL·min^{-1}. This means that, despite the (slight) increase in yields, as the reactant flowrates are smaller, lesser amounts of water are formed that can be adsorbed into the zeolite. Thus, working at a *WHSV* of 1.5 × 10^4 (STP) mL·g$^{-1}_{cat}$·h^{-1} (or 4.86 g_{CO2}·g$^{-1}_{cat}$·h^{-1}) results in the generation of greater amounts of water, which can then be adsorbed and removed from the reaction environment. As such, this value is the one where there is more room to achieve process intensification and analyze the influence of other parameters. Therefore, this value of *WHSV* was set as a reference in further experiments.

3.2. Effect of temperature in reaction performance

The following study was focused on determining the influence of temperature in the process intensifications. Thus, the temperature value was modified in reaction experiments, from 250 to 400 °C, while keeping a constant *WHSV* of 1.50 × 10^4 (STP) mL·g$^{-1}_{cat}$·h^{-1}. In this situation, two opposite trends meet; on the one hand, a higher temperature should result in faster reaction kinetics, leading to increased yields to methane and a greater formation of water which is removed by the zeolite. On the other hand, as adsorption is an exothermic process, it is favored by lower temperatures. For this reason, it is necessary to determine an optimal value, which brings the greatest process intensifications. Fig. 3 shows the results achieved at all four different temperatures, while Table 4 depicts process intensifications, in terms of water adsorbed per adsorbent weight and in relative performance over the stable value (Table 4).

The experiments demonstrate that reaction temperature does indeed affect the achieved intensifications. As shown in Fig. 3, a lower temperature is related to an earlier saturation of the zeolite. Thus, a stable value of yields ($Y_{CO_2 \rightarrow CH_4}$ = 0.16 in *T* = 250 °C) is reached much more quickly than at higher temperatures (i.e., at 350 °C yields do not stabilize in the first reaction stage M_1, and instead, they do in the second stage M_2, at $Y_{CO_2 \rightarrow CH_4}$ = 0.70). Since water adsorption is most favored at 250 °C, at this temperature the maximal relative intensifications are reached, and the reaction equilibrium is most modified towards products formation. These intensifications then decrease as the temperature rises.

The other extreme is reached at 400 °C. When operating at this temperature, not only is water adsorption less favored than at lower values, but the stable yields are already very close to thermochemical equilibrium ($Y_{CO_2 \rightarrow CH_4}$ = 0.83). This leaves less room to reach an intensification, which is the lowest in value of all four temperatures; in addition, the stable situation is reached almost at the beginning –after five minutes of time on stream–, while at 250 °C it still takes approxi-

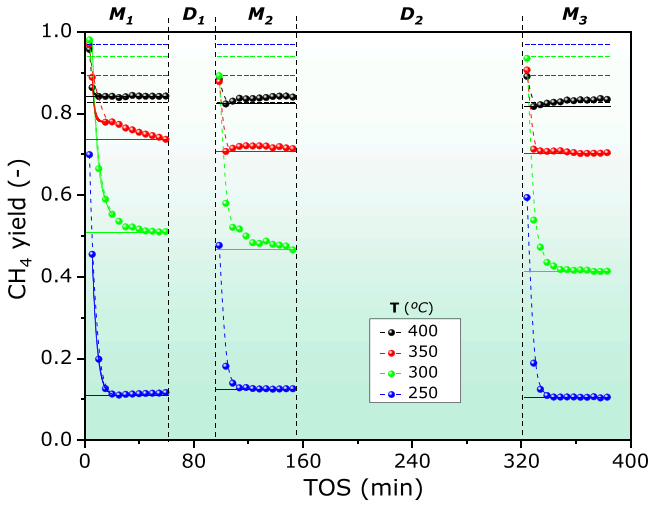

Fig. 3. Methane yield ($Y_{CO_2 \rightarrow CH_4}$) at different temperatures along methanation (M) + desorption (D) experiments. H_2:CO_2 ratio= 4:1. Reactants: Inert ratio = 9:1. *WHSV* = 1.50×10^4 (STP) mL·g$^{-1}_{cat}$·h^{-1}. Total bed load: 10.5 g. Dashed lines represent thermodynamic equilibrium conversion calculated by ΔG minimization.

Table 4
Specific and relative water intensifications (Eqs. 5 and 6, respectively) as a function of temperature.

		Specific intensification (mmol H_2O/kg zeolite)			
	T (°C)	*400*	*350*	*300*	*250*
Reaction stages	M_1	94.6	884.7	1335.5	932.7
	M_2	324.4	363.5	1063.8	491.2
	M_3	338.4	281.1	950.4	707.6
		Relative intensification (-)			
	T (°C)	*400*	*350*	*300*	*250*
Reaction stages	M_1	1.005	1.055	1.121	1.389
	M_2	1.019	1.025	1.109	1.188
	M_3	1.018	1.018	1.101	1.300

mately 20 minutes to saturate.

However, when considering the amounts of water adsorbed into the zeolite, the optimal operating temperature is found at 300 °C. This is due to the fact that, when working at this space velocity, yields to methane reach relatively high values –around $Y_{CO_2 \rightarrow CH_4} = 0.50$. This, combined with adsorption being favored, allows the removal of water and increases the reaction performances, even going beyond thermochemical constraints at the beginning of M_1 and M_3, when the zeolite is fresh and has not been exposed to water, in M_1, and when the desorption process is effective enough to allow the adsorption of new water molecules, in M_3.

It is necessary to consider, however, that stable values in M_3 ($Y_{CO_2 \rightarrow CH_4} = 0.41$) are clearly lower than those obtained in M_1 ($Y_{CO_2 \rightarrow CH_4} = 0.51$) and M_2 ($Y_{CO_2 \rightarrow CH_4} = 0.48$), which points out that might be some loss of activity withing the bed, which results in a decrease of reaction performance over time. This contrasts with previous tests, where it was shown that the catalyst was stable after 70 hours in operation and is attributed to the presence of zeolite in the catalytic bed. While its low Si/Al ratio favors water affinity and adsorption, it also makes it more acid and might favor coke formation, which was detected in additional experiments although at an extremely low extent. Sintering was also observed, due to the high temperatures (500 °C in D_2), presence of water as a strong oxidant, and the fact that nickel is one of the active phases of the catalyst. As Fig. 3 shows, some loss of activity in the solid conforming the bed takes place gradually and increases over time, since differences between results become stronger as the experiment develops (i.e., yields are lower in M_3 than in M_2, and these lower than in M_1).

It can be observed that, as opposed to what could be expected, at 300 °C minimal intensifications are reached in the third methanation stage (M_3), while they become maximal in M_1 (just as predicted) and intermediate in M_2. Meanwhile, at 250 °C the maximal values (both relative and in terms of amounts of water) are obtained in M_1. This can be explained as another effect of loss of activity of the mixture of solids conforming the bed; since it modifies stable values, it might interfere with them (since they are taken as a reference to calculate intensifications) and alter the results that would be observed if only reaction kinetics and adsorption processes were at work.

An additional issue lies in the fact that, as a fixed bed reactor, there is a temperature profile along the bed. Thus, in order to analyze its effect on reaction performance, it was registered with the aid of five thermocouples located at its axis (see Fig. 1). Analysis verified that a high degree of isothermicity was achieved, and that, while not nonexistent, temperature gradients were smoother than five degrees in the whole bed before the beginning of the experiment (for a better visualization, at zero time, the hottest spot located at 9 cm was 349.5 °C, while the coldest spot was 346 °C).

After that, the temperatures rose, due to the fact that the reaction front was reaching the different bed heights, creating a transient state before the final stabilization of the system. At this moment, maximal temperatures reached a value of 374 °C in the hot spot (at the highest point in the reactor) before finally stabilizing at 364 °C, with a cold spot of 344 °C. Thus, the stable temperature profile is registered to be 20 °C. A map with different temperatures, at the beginning of a methanation stage until reaching a steady state (time on stream equal to 15 minutes), is shown in Fig. 4.

Another way to measure the intensification lies in comparing the results obtained with those at a stable state, in absence of intensifications. Thus, the yields were divided by those at the end of stages, confirming that the same trends observed in relative intensifications are present (stabilized values normalized to ×1). These quotients are observed in Fig. 5.

From the graphics in Fig. 5, it is confirmed once again that the relative improvements are greatest at 250 °C, following in decreasing order of temperatures. Taking 1 as the arbitrary stable value, it can be seen that improvements rise up to 6 at the beginning of M_1 at 250 °C, following by around 2 at 300 °C, 1.25 at 350 °C, and 1.10 at 400 °C. This takes place not only because of adsorption being favored at low temperatures, but also because stable yields are smaller (i.e., $Y_{CO_2 \rightarrow CH_4} = 0.15$ at 250 °C and $Y_{CO_2 \rightarrow CH_4} = 0.85$ at 400 °C) and thus less water is formed, taking more time for the zeolite to saturate.

Although the quotients evolve in the same way among the four temperatures tested (higher quotients at 250 and lower at 400 °C), contrary to the expected results, saving for 250 °C, improvements are maximal at M_3. It becomes particularly pronounced at 350 °C -being of 2.22 at M_3 and 1.92 at M_1-. This further confirms that a loss of intensification is present in the experiments, as while initial values are approximately constant, yields are lower in the third stage, which interferes in the final results.

It is concluded then that among all temperatures tested, 300 °C is the best one, reaching both high yields to methane and strong displacement of equilibrium due to adsorption. Working at 250 °C favors water adsorption to a greater degree –but reaction kinetics are too slow to allow the achievement of high yields towards methane, ultimately resulting in yields that are no higher than 0.50, while (initially) achieving more than 0.90 at 300 °C. The opposite happens at 350 and 400 °C; although stable values are clearly higher than those obtained at 300 °C, water adsorption is less favored, which combined with the fact that reaction performances are already close to equilibrium, leave less room to improvement and intensification.

3.3. Biogas feeding

Once the influence of temperature has been tested with a diluted carbon dioxide feeding, the next step consisted of repeating the same experiment conditions with a synthetic sweetened biogas (containing

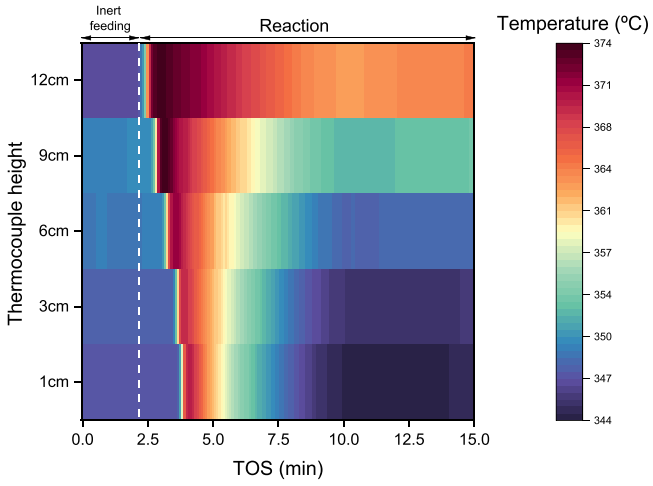

Fig. 4. Temperature profiles along the catalytic fixed bed, at the beginning of the methanation stage M_1. T = 350 °C. H_2:CO_2 ratio= 4:1. Reactants: Inert ratio = 9:1. $WHSV = 1.50 \times 10^4$ (STP) mL·g_{cat}^{-1}·h^{-1}. Total bed load: 10.5 g.

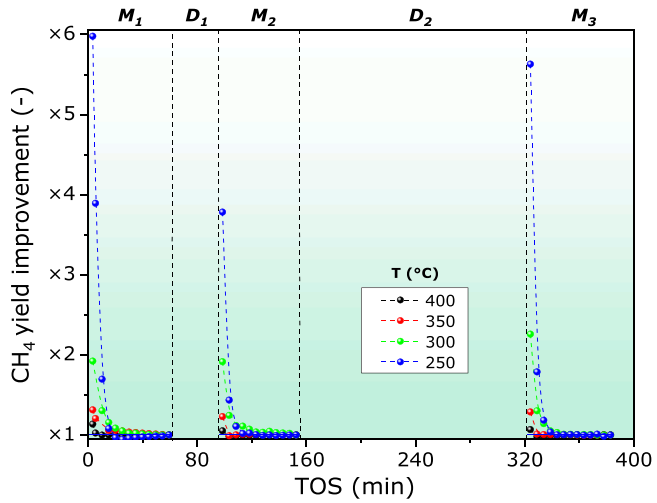

Fig. 5. Improvements in methane yields ($Y_{CO_2 \rightarrow CH_4}$) at different temperatures along methanation (M) + desorption (D) experiments. Stable values: normalized to 1. H_2:CO_2 ratio= 4:1. Reactants: Inert ratio = 9:1. *WHSV* = 1.50×10^4 (STP) mL·g_{cat}^{-1}·h^{-1}. Total bed load: 10.5 g.

70 ^{v}% methane and 30 ^{v}% carbon dioxide) in order to check the effect of processing this raw material. Although it was expected that yields to methane will be affected to some degree, it has been proven that except for 400 °C –where equilibrium tends to favor coke and carbon monoxide production- the results are not greatly influenced by the *Le Châtelier* principle. The results, at different temperatures, for biogas feeding are shown in Fig. 6.

It is now confirmed that, saving for the highest temperature (400 °C), differences between comparable feedings of biogas and carbon dioxide are very small. For example, at the temperature of 300 °C, the results are kept constant at around $Y_{CO_2 \rightarrow CH_4} = 0.5$, which demonstrates that presence of methane has a very small effect on reaction and that it is not necessary to remove it from the environment in order to achieve a similar result.

At 400 °C, nevertheless, it is shown that yields decrease from 0.8 to 0.75, which can be explained as the effect of thermochemical equilibrium disfavoring methane generation. However, it was previously stated that at this temperature intensifications are nonexistent and thus it is not

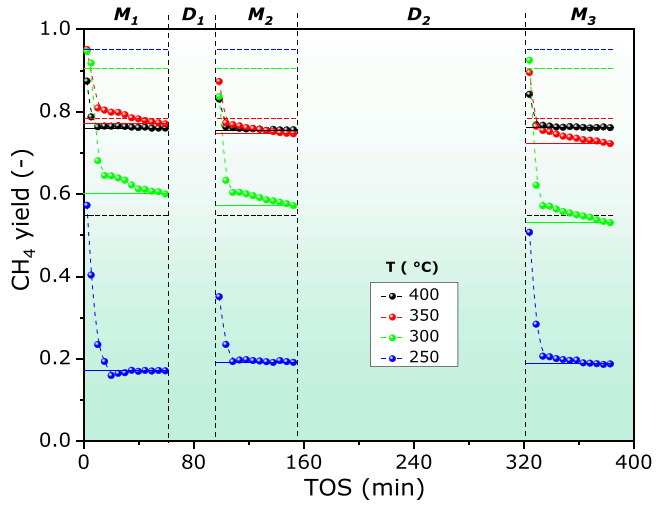

Fig. 6. Methane yield ($Y_{CO_2 \rightarrow CH_4}$) at different temperatures along methanation (M) + desorption (D) experiments. CH_4:CO_2 ratio= 7:3. H_2:CO_2 ratio = 4:1. Reactants: Inert ratio = 9:1. *WHSV* = 1.50×10^4 (STP) mL·g_{cat}^{-1}·h^{-1}. Total bed load: 10.5 g. Dashed horizontal lines represent thermodynamic equilibrium conversions calculated by ΔG minimization.

interesting to operate in those conditions. Table 5 shows the intensification values.

It is confirmed that, unlike what happened in the experiments without methane, relative intensifications are maximal at 250 °C for all three methanation stages. Since a lower temperature favors adsorption, it becomes stronger at 250 °C and intensifications are higher. For specific intensifications, however, which take into account the amounts of water that are formed in the reaction, the best temperature switches from 250 to 300 °C. Since relative intensifications are not too different from each other (i.e., they are 1.09 at 300 and 1.19 at 250 °C for M_1), while the yields are clearly higher ($Y_{CO_2 \rightarrow CH_4} = 0.6$ vs. $Y_{CO_2 \rightarrow CH_4} = 0.15$), greater amounts of water are generated and adsorbed, and specific intensifications become higher.

After comparing the improvements, however, it is clearly shown that they are lower than those with carbon dioxide feeding. Fig. 7 depicts the results.

Unlike what happened in previous results, improvements have decreased sharply, from 6 to 3.4 for the maximal value -which is reached in M_1 at 250 °C. Although stable yields are similar to those without methane, it must be considered that carbon dioxide flowrates are smaller; thus, fewer amounts of water are formed, and intensifications are achieved to a lesser degree.

What remains from previous experiments, however, is that -except at 250 °C-, maximal improvements are met in M_3. For example at 300 °C, improvements are 1.75 in M_3, while M_1 values are no higher than 1.60. This confirms that there is a decrease of activity during the course of an experiment and that the catalyst is not stable after three methanation and two desorption stages.

3.4. Partial pressures of reactants

The last parameter tested is the partial pressure of reactants, modifying the H_2:CO_2 molar ratio from 2:1 to 6:1. The expected outcome was that, as the number of H_2 molecules (1 mol) that participate in CO generation (r.2) is different than that of methane formation (4 moles) (r.1), working in excess of this reactant may increase CH_4 production, thus favoring the formation of more water molecules and its subsequent adsorption. The evolution of results when carrying out experiments at different partial pressures is displayed in Fig. 8.

In this last case, it is confirmed that carbon dioxide conversions, along with methane yields, rise when operating with an excess of hydrogen (overstoichiometric ratios) and become lower when operating at substoichiometric ratios (2:1). In fact, since the number of molecules of hydrogen is different in the formation of both products, not only are carbon dioxide conversions affected, but also selectivity towards methane, further increasing yields, which are well above 0.9 while working at 6:1.

Moreover, it is shown that, when hydrogen is introduced in excess, yields tend to stabilize at later times than when it is fed in defect. This phenomenon is taking place due to the fact that greater amounts of

Table 5
Specific and relative water intensifications (Eqs. 5 and 6, respectively) as a function of temperature (biogas).

	Specific intensification (mmol H_2O/kg zeolite)				
	T (°C)	*400*	*350*	*300*	*250*
Reaction stages	M_1	162.5	666.6	1250.7	711.3
	M_2	138.8	357.2	701.1	290.1
	M_3	126.4	548.6	972.7	640.1
	Relative intensification (-)				
	T (°C)		*400*	*350*	*300*	*250*
Reaction stages	M_1		1.010	1.039	1.094	1.189
	M_2		1.009	1.023	1.059	1.072
	M_3		1.007	1.033	1.081	1.150

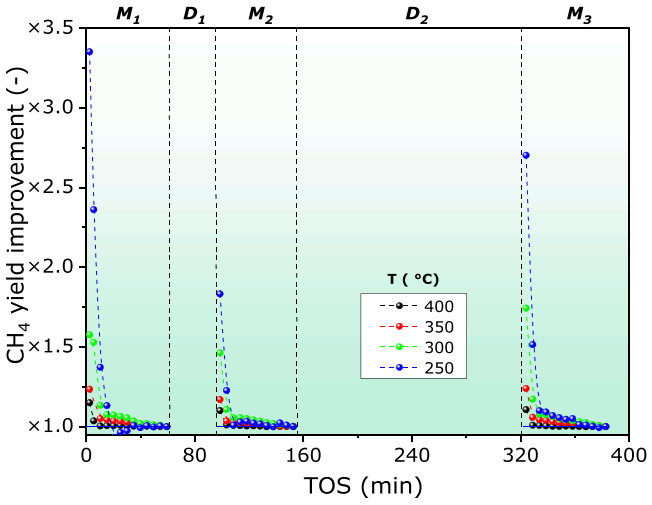

Fig. 7. Improvements in methane yields ($Y_{CO_2 \to CH_4}$) at different temperatures along methanation (M) + desorption (D) experiments, with a biogas feeding. Stable values: normalized to 1. CH_4:CO_2 ratio= 7:3. H_2:CO_2 ratio = 4:1. Reactants: Inert ratio = 9:1. *WHSV* = 1.50×10^4 (STP) mL·g_{cat}^{-1}·h^{-1}. Total bed load: 10.5 g.

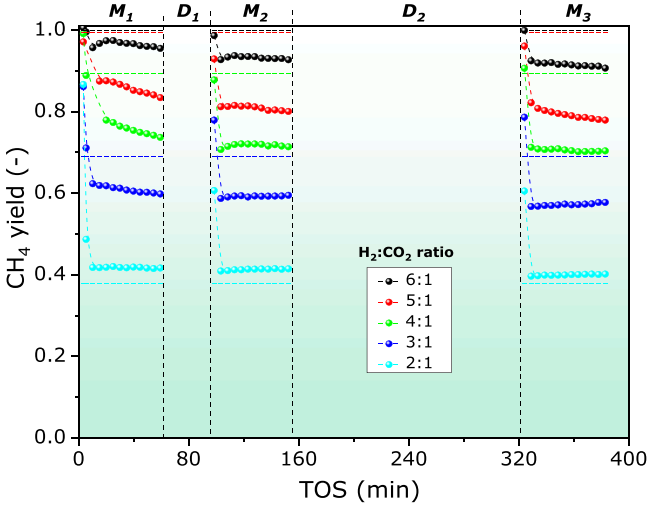

Fig. 8. Methane yield ($Y_{CO_2 \to CH_4}$) at different partial pressures along methanation (M) + desorption (D) experiments. T = 350 °C. Reactants: Inert ratio = 9:1. *WHSV* = 1.50×10^4 (STP) mL·g_{cat}^{-1}·h^{-1}. Total bed load: 10.5 g. Dashed horizontal lines represent thermodynamic equilibrium conversion calculated by ΔG minimization.

water are formed, which then adsorb into the zeolite, displacing the reaction equilibrium. However, working in excess of carbon dioxide results in an increase of carbon monoxide formation and lower conversions. Thus, less water is formed, and adsorption becomes less intense, resulting in a milder degree of intensification. Table 6 displays the achieved intensifications, as a function of partial pressures.

From these results, it can be extracted that, in terms of relative intensification, for the first stage (M_1) the optimal values are reached when working at ratios 5:1 and 4:1. This is chalked up to the fact that a high concentration of H_2 favors higher conversion of carbon dioxide, as well as selectivity towards methane. Nevertheless, it should also be considered that, while modifying partial pressures, carbon dioxide flowrates also change. Even though working at an excess of hydrogen allows greater yields to methane, lower flows of this reactant limit water formation, which then results in a lower adsorption. Thus, while the highest yields are reached at 6:1, intensifications are lesser than those

Table 6
Specific and relative water intensifications (Eqs. 5 and 6, respectively) as a function of partial pressures.

		Specific intensification (mmol H_2O/kg zeolite)				
	H_2:CO_2 (-)	*6:1*	*5:1*	*4:1*	*3:1*	*2:1*
Reaction stages	M_1	276.3	799.6	998.6	486.8	288.9
	M_2	155.3	300.3	221.6	120.3	146.4
	M_3	285.2	504.4	233.9	79.6	146.0
		Relative intensification (-)				
	H_2:CO_2 (-)	*6:1*	*5:1*	*4:1*	*3:1*	*2:1*
Reaction stages	M_1	1.013	1.044	1.063	1.038	1.032
	M_2	1.008	1.018	1.015	1.010	1.017
	M_3	1.014	1.028	1.015	1.006	1.016

obtained at 5:1. The same trend is observed when comparing the results at 4:1, where the maximal water adsorption takes place.

The optimal conditions vary in the second (M_2) and third (M_3) methanation stages, however. This happens in situations where the zeolite has already adsorbed water and thus is not fresh. As such, some water has not been desorbed during desorption steps (D_i) and it affects later performances. When operating at 4:1 (the optimal previous situation) a greater degree of water adsorption leads to difficulties when removing it in the first desorption stage (D_1), which takes place at the same reaction temperature -where it was theorized that adsorption, the reverse process, is strongly favored. In the second stage, the optimal ratio is found to be 5:1 (where a compromise between high yields to methane and more room to adsorb water is met), while 4:1 falls to the second place, having high yields to methane and a high flow, but less capacity to adsorb the new water molecules.

Finally, in the third reaction stage (M_3), the ratio 5:1 stands as the optimal situation once again. While the first desorption stage took place at the reaction temperature (350 °C), in the second one (D_2) temperature rose to 500 °C, favoring water desorption and removal. However, the zeolite is still not completely regenerated, so there is still presence of water on it to some extent. In these circumstances, the ratio 5:1 (with its lower water generation and adsorption) is related to a smaller degree of saturation than 4:1. In fact, it can be seen that differences in results are greater in M_3 than in M_2 (as the values are 300.3 and 221.6 in M_2 and 504.4 and 233.9 in M_3), further confirming that the presence of water in the zeolite is stronger when operating in 4:1. Thus, the ratio 5:1 stands as the most adequate as the compromise between yields to methane and water formation.

4. Conclusions

This study demonstrates the effectiveness of integrating catalytic methanation with adsorption processes to enhance methane production from CO_2 hydrogenation. By leveraging a Ni-Fe-based catalyst combined with LTA 5 A zeolite, the work addresses key challenges associated with the *Sabatier* reaction, including thermodynamic equilibrium limitations and the adverse effects of water accumulation. The ability of zeolite to *in situ* adsorb water proved pivotal, enabling the intensification of methane production and yielding efficiencies that exceed thermodynamic predictions in the initial stages of the reaction. These findings validate the *Sorption-Enhanced Methanation* (SEM) concept as a practical approach to optimize CO_2 utilization technologies.

Optimal operating conditions were identified, with a temperature of 300 °C, a *WHSV* of 1.50×10^4 (STP) mL·g_{cat}^{-1}·h^{-1}, and a H_2:CO_2 molar feed ratio equal to 5:1 delivering the highest methane yields under the studied configurations. These conditions not only enhanced catalytic performance but also maintained compatibility with the thermodynamic constraints of the reaction. However, substoichiometric ratios (e.g., 2:1) shifted selectivity toward carbon monoxide, leading to lower methane yields and reduced water formation, which subsequently weakened the

adsorption-driven intensifications. These results confirmed that an excess of hydrogen not only drives higher methane production, but also promotes water adsorption, thus maximizing reaction efficiency. Furthermore, the study confirmed that the presence of methane in the feed stream -simulating biogas upgrading to *synthetic natural gas*- did not compromise the reaction process, making this approach suitable for direct biogas upgrading applications. This insight positions the combined catalytic-adsorptive system as a viable technology for production of renewable methane while leveraging existing biogas resources.

One of the challenges identified in the experiments was the mild but gradual loss of activity of the solid bed conformed by the catalyst itself and the water adsorbent (LTA 5 A zeolite), observed during prolonged operation. This phenomenon has been attributed to the accumulation of water inside the zeolite despite successive desorption stages based on inert gas flow and increased temperatures. Although it has not been confirmed, the possibility of coke formation due to the acidic nature of the zeolites (low Si/Al ratio) could be another contributing phenomenon leading to the progressive loss of activity in the bed. Additionally, sintering effects and nickel oxidation might be exacerbated by the reaction plus desorption conditions, including high temperatures and water exposure. These deactivation phenomena resulted in declining performance over successive reaction stages, particularly at higher temperatures.

In summary, this work establishes a foundation for adsorption-enhanced methanation as an advanced method for CO_2 valorization, with significant implications for energy storage and carbon management. The combination of Ni-Fe catalysts with LTA 5 A zeolites represents a promising route for achieving high methane yields while mitigating the limitations of conventional methanation processes.

CRediT authorship contribution statement

Víctor Daniel Mercader: Writing – review & editing, Writing – original draft, Methodology, Investigation, Formal analysis. **Pablo Aragüés-Aldea:** Writing – review & editing, Writing – original draft, Investigation, Formal analysis, Data curation. **Paúl Durán:** Writing – review & editing, Resources, Methodology, Conceptualization. **Eva Francés:** Writing – review & editing, Methodology, Conceptualization. **Javier Herguido:** Writing – review & editing, Visualization, Supervision, Methodology, Formal analysis, Conceptualization. **Jose-Angel Peña:** Writing – review & editing, Supervision, Project administration, Methodology, Funding acquisition, Formal analysis, Conceptualization.

Declaration of Competing Interest

The authors declare that they have no known competing financial interests or personal relationships that could have appeared to influence the work reported in this paper.

Acknowledgements

This research has been funded by MICINN (*Spanish Ministerio de Ciencia e Innovación*) project number PID2022–136947OB-I00 and European Union Next Generation PRTR-C17.I1 Task LA4.A1. Additionally, the consolidated research group Catalysis and Reactor Engineering Group (CREG) (T43–23R) has received financial support from *Gobierno de Aragón* (Aragón, Spain) through the European Social Fund – FEDER. In addition, P. Aragüés-Aldea and V. D. Mercader (grant no. PRE2020–095679) express their gratitude for the research predoctoral grants of Gobierno de Aragón and Spanish Ministerio de Ciencia e Innovación respectively. Lastly, authors also acknowledge the work of *Servicio General de Apoyo a la Investigación-SAI* (Universidad de Zaragoza).

Data availability

Data will be made available on request.

References

[1] F. Kourougianni, et al., A comprehensive review of green hydrogen energy systems, Renew. Energy 231 (Sep. 2024) 120911, https://doi.org/10.1016/j.renene.2024.120911.
[2] P.E. Dodds, S.D. Garvey, Energy storage options to balance renewable electricity systems, Elsevier eBooks, 2022, pp. 13–33, https://doi.org/10.1016/b978-0-12-824510-1.00032-5.
[3] M. Noussan, V. Negro, M. Prussi, D. Chiaramonti, The potential role of biomethane for the decarbonization of transport: an analysis of 2030 scenarios in Italy, Appl. Energy 355 (Nov. 2023) 122322, https://doi.org/10.1016/j.apenergy.2023.122322.
[4] CORDIS – European Commission, "Power-to-gas system enables massive storage of renewable energy [Online]. Available, Eur. Union H2020 (2020), https://doi.org/10.3030/717957.
[5] A.H. Hatta, et al., A short review on informetric analysis and recent progress on contribution of ceria in Ni-based catalysts for enhanced catalytic CO methanation ([Online]. Available), Powder Technol. 417 (2023) 118246, https://doi.org/10.1016/j.powtec.2023.118246.
[6] A. Bermejo-López, B. Pereda-Ayo, J.A. Onrubia-Calvo, J.A. González-Marcos, J. R. González-Velasco, Enhancement of the CO_2 adsorption and hydrogenation to CH_4 capacity of Ru–Na–Ca/γ–Al_2O_3 dual function material by controlling the Ru calcination atmosphere, J. Environ. Sci. 140 (2024) 292–305, https://doi.org/10.1016/j.jes.2023.08.041.
[7] C. Di Stasi, et al., Optimization of the operating conditions for steam reforming of slow pyrolysis oil over an activated biochar-supported Ni–Co catalyst ([Online]. Available), Int. J. Hydrog. Energy 46 (53) (2021) 26915–26929, https://doi.org/10.1016/j.ijhydene.2021.05.193.
[8] L. Wei, W. Haije, H. Grénman, W. De Jong, Sorption enhanced catalysis for CO_2 hydrogenation towards fuels and chemicals with focus on methanation, Elsevier eBooks, 2022, pp. 95–119, https://doi.org/10.1016/b978-0-323-85612-6.00004-8.
[9] E. Mancusi, G. Piso, H.H. Shah, F. Pepe, C. Tregambi, P. Bareschino, Modelling of a continuous sorption-enhanced methanation process in an adiabatic packed-bed reactor system, Chem. Eng. Sci. 301 (2025) 120800, https://doi.org/10.1016/j.ces.2024.120800.
[10] M. Tommasi, S.N. Degerli, G. Ramis, I. Rossetti, Advancements in CO_2 methanation: a comprehensive review of catalysis, reactor design and process optimization, Process Saf. Environ. Prot. 201 (Dec. 2023) 457–482, https://doi.org/10.1016/j.cherd.2023.11.060.
[11] S. Renda, C. Di Stasi, J.J. Manyà, V. Palma, Biochar as support in catalytic CO_2 methanation: enhancing effect of CeO_2 addition, *J. CO_2 Util.* 53 (Nov. 2021) 101740, https://doi.org/10.1016/j.jcou.2021.101740.
[12] O.E. Medina, A.A. Amell, D. López, A. Santamaría, Comprehensive review of nickel-based catalysts advancements for CO_2 methanation, Renew. Sustain. Energy Rev. 207 (Sep. 2024) 114926, https://doi.org/10.1016/j.rser.2024.114926.
[13] D. Pandey, G. Deo, Effect of support on the catalytic activity of supported Ni–Fe catalysts for the CO_2 methanation reaction, J. Ind. Eng. Chem. 33 (Sep. 2015) 99–107, https://doi.org/10.1016/j.jiec.2015.09.019.
[14] L. Gómez, I. Martínez, M.V. Navarro, R. Murillo, Selection and optimisation of a zeolite/catalyst mixture for sorption-enhanced CO_2 methanation (SEM) process, *J. CO_2 Util.* 77 (Oct. 2023) 102611, https://doi.org/10.1016/j.jcou.2023.102611.
[15] L. Wei, H. Azad, W. Haije, H. Grenman, W. De Jong, Pure methane from CO_2 hydrogenation using a sorption enhanced process with catalyst/zeolite bifunctional materials, Appl. Catal. B Environ. Energy 297 (Jun. 2021) 120399, https://doi.org/10.1016/j.apcatb.2021.120399.
[16] A.A. Abd, M.R. Othman, Z. Helwani, J. Kim, An overview of biogas upgrading via pressure swing adsorption: navigating through bibliometric insights towards a conceptual framework and future research pathways, Energy Convers. Manag. 306 (Mar. 2024) 118268, https://doi.org/10.1016/j.enconman.2024.118268.
[17] V.D. Mercader, P. Durán, P. Aragüés-Aldea, E. Francés, J. Herguido, J.Á. Peña, Biogas upgrading by intensified methanation (SESaR): reaction plus water adsorption - desorption cycles with Ni-Fe/Al_2O_3 catalyst and LTA 5A zeolite, Catal. Today 433 (Mar. 2024) 114667, https://doi.org/10.1016/j.cattod.2024.114667.
[18] A. Sanz-Martínez, P. Durán, V.D. Mercader, E. Francés, J.Á. Peña, J. Herguido, Biogas upgrading by CO_2 methanation with Ni-, Ni–Fe-, and Ru-based catalysts, Catalysts 12 (12) (Dec. 2022) 1609, https://doi.org/10.3390/catal12121609.
[19] L. Gómez, I. Martínez, G. Grasa, R. Murillo, Experimental demonstration of a sorption-enhanced methanation (SEM) cyclic process on a lab-scale TRL-3 fixed bed reactor, Chem. Eng. J. 491 (Jul. 2024) 151744, https://doi.org/10.1016/J.CEJ.2024.151744.
[20] A. Cañada-Barcala, M. Larriba, V.I. Águeda Maté, J.A. Delgado Dobladez, Synthetic natural gas production through biogas methanation using a sorption-enhanced reaction process, Sep. Purif. Technol. 331 (Mar. 2024) 125714, https://doi.org/10.1016/j.seppur.2023.125714.